# Vehicle Suspension Relative Velocity Estimation Using a Single 6-D IMU Sensor

Kicheol Jeong and Seibum B. Choi, *Member, IEEE*

***Abstract*—This paper proposed a method for estimating the suspension relative velocity using a single six-dimensional measurement unit attached to a vehicle body. This method can reduce the number of sensors, reduce costs, and address sensor packaging issues. A wheelbase preview assumption is used to overcome the lack of unsprung mass information. The proposed estimation method is verified by the vehicle simulator Carsim and the stability of the estimation method is also analyzed. In addition, the frequency response and the time response of the sky-hook controller based on the estimated relative velocity are compared with the sky-hook controller based on the actual relative velocity. The results show that the proposed estimator produces very robust performance on various road conditions.**

***Index Terms*—Suspension relative velocity, wheelbase preview, 6-D IMU, neutral type delay system.**

## I. Introduction

SUSPENSION systems are the main components of a vehicle that determine ride comfort and handling performance. Since passive suspension has unchanged damping characteristics, it is difficult to satisfy both handling and riding comfort, which conflict with each other [1]. To solve this problem, active and semi-active suspensions [2], [3] that change damping characteristics according to vehicle conditions have been proposed over the past three decades. In particular, semi-active suspension is used more extensively than active suspension in order to address energy and packaging issues. Thus far, various types of control strategies [4]–[9] have been developed to improve the performance of semi-active suspensions. However, in most semi-active suspension control studies, it is assumed that the state of the suspension is known. For example, the sky-hook control [7], [10], [11], which is widely used in practical applications, requires the suspension relative velocity to determine the damping command. The suspension relative velocity is thus essential information in the suspension control area. For cost effectiveness and packaging optimization, the suspension relative velocity should be estimated from other measurements. For this reason, various methods for estimating the suspension relative velocity have been studied. Kyoungsu Yi [12], [13] proposed a disturbance decoupled observer to avoid the effects of unknown road disturbances. To cope with unknown road input, Dugard [14] developed a full car model based vehicle vertical state estimator using the H-inf criterion. Dixit [15] proposed a sliding mode observation using a nonlinear reference model. Kalman filtering [16], [17] was also used to estimate the relative velocity between vehicle sprung and unsprung mass. Hernandez [18] compared several estimation methods such as an integrator, Luenberger observer, and unknown input observer. A common feature of the methods studied thus far is the use of a sensor system consisting of sprung mass sensors and unsprung mass sensors. Indeed, most estimation methods use an accelerometer and a position sensor, or two accelerometers, which are located on the vehicle body and the wheel house of a vehicle. However, the sensors used in these estimation methods, especially the wheel acceleration sensors or displacement sensors located in the wheel housings, have problems such as packaging and sensor defects due to road impurities. In addition, when using these estimation methods, sensors are attached to every corner, which increases the cost and effort for vehicle production.

In this paper, the authors introduce a novel method for estimating the relative velocity of a vehicle suspension system using a single six-dimensional measurement unit (6-D IMU). The advantage of this method is that there is no packaging problem of the wheel acceleration sensor or position sensor. While 6-D IMU sensor are relatively more expensive than accelerometers, this sensor can replace five vertical accelerometers. In addition, 6-D IMU contains vehicle longitudinal acceleration, lateral acceleration and yaw rate information. Therefore, the vehicle does not require additional sensors for electronic stability control (ESC). As a result, 6-D IMU sensor substitute five single axis accelerometers and one ESC sensor. Indeed, the cost and effort of configuring the sensor system can be reduced significantly. The suggested estimation method is introduced as follows. First, the governing equations are derived from a full car model. Since the number of governing equations is not sufficient to obtain the information on the four corners of the vehicle, additional constraints are introduced using the wheelbase preview assumption. Next, the relative speed estimation method is introduced in four steps. In addition, stability of the estimator is verified. Finally, this method is verified using a commercial vehicle simulator Carsim. To verify the practicality of the estimation method, the frequency response and the time response

Manuscript received September 13, 2018; revised January 4, 2019; accepted May 26, 2019. Date of publication June 5, 2019; date of current version August 13, 2019. This work was supported in part by the Technology Innovation Program (or Industrial Strategic Technology Development Program under Grant 10084619, Development of Vehicle Shock Absorber (Damper) and Engine Mount Using MR Fluid with Yield Strength of 60kPa) funded by the Ministry of Trade, Industry & Energy (MOTIE, Korea); and in part by the BK21+ Program through the National Research Foundation funded by the Ministry of Education of Korea. The review of this paper was coordinated by Dr. S. Anwar. *(Corresponding author: Seibum B. Choi.)*

The authors are with the Korea Advanced Institute of Science and Technology, Daejeon 34141, South Korea (e-mail: cbrxxiq@kaist.ac.kr; sbchoi@kaist.ac.kr).

Digital Object Identifier 10.1109/TVT.2019.2920876

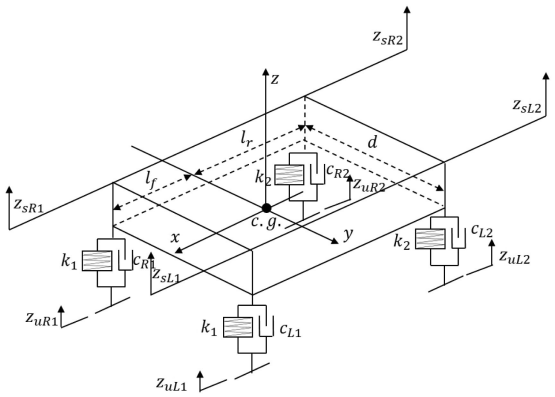


Fig. 1. Free body diagram of the vehicle body.

of the sky-hook controller based on the estimated relative velocity are compared with the sky-hook controller based on the actual relative velocity obtained by Carsim. In conclusion, this paper shows that the proposed method provides very robust performance in various road conditions such as speed bumps and wavy roads.

## II. Vehicle Model and Wheelbase Preview Assumption

This section proposes a full car model for estimating suspension relative speeds. In addition, a wheelbase preview assumption is introduced to estimate the relative velocity using a single 6-D IMU.

### A. Vehicle Model and Governing Equations

The purpose of this study is to estimate the relative velocity of four suspensions using one sensor attached to the vehicle body. This sensor system is able to detect the movement of the vehicle body, but there is a limitation that the information of the unsprung mass cannot be known independently. Therefore, it is reasonable to estimate the relative velocity based on the vertical force acting on each corner of the vehicle body. Fig. 1 shows a free body diagram of the vertical force acting on the vehicle body based on a full car model [8], [19]–[21] and Table I describes the vehicle properties.

According to Fig. 1, three governing equations for the vertical motion of the vehicle are obtained from 6-D IMU measurements.

$$\begin{cases} m_s a_z(t) = F_{L1}(t) + F_{L2}(t) + F_{R1}(t) + F_{R2}(t) \\ I_x \dot{p}(t) = \frac{d}{2}\left(F_{L1}(t) + F_{L2}(t)\right) - \frac{d}{2}\left(F_{R1}(t) + F_{R2}(t)\right) \\ I_y \dot{q}(t) = l_r\left(F_{L2}(t) + F_{R2}(t)\right) - l_f\left(F_{L1}(t) + F_{R1}(t)\right) \end{cases} \tag{1}$$

where $F_{L1}(t), F_{L2}(t), F_{R1}(t)$ and $F_{R2}(t)$ are suspension force and $a_z(t), p(t)$ and $q(t)$ are sensor measurements that represent vertical acceleration, roll and pitch rate of vehicle mass centre. (1) is a set of governing equations representing heave, roll, and pitch behaviour of the vehicle body. However, based on the 6-D IMU, only three governing equations can be obtained, even though the number of required information is four. Therefore, additional constraints are necessary to solve this underdetermined problem.

TABLE I
Vehicle Properties

| Symbol | Quantity | Value |
|---|---|---|
| $m_s$ | Sprung mass | 1370 kg |
| $I_x$ | Roll inertia | 671.3 $kgm^2$ |
| $I_y$ | Pitch inertia | 1972.8 $kgm^2$ |
| $k_1$ | Front spring stiffness | 153000 N/m |
| $k_2$ | Rear spring stiffness | 82000 N/m |
| $c_{R1}$,$c_{L1}$ | Front right and left damping coefficient | Variable |
| $c_{R2}$,$c_{L2}$ | Rear right and left damping coefficient | Variable |
| $d$ | Distance from left to right wheel | 1.55 m |
| $l_f$ | Distance from C.G. to front wheel | 1.11 m |
| $l_r$ | Distance from C.G. to rear wheel | 1.67 m |

### B. Wheelbase Preview Assumption

To cope with insufficient governing equations, a wheelbase preview assumption [6], [9] is introduced in this section. Assuming that the lateral movement of the vehicle is negligible, the rear wheels pass through the same road profile that the front wheels have already passed with a certain time gap. This time interval is the wheelbase divided by the vehicle velocity. This is a reasonable assumption, except for differences in tire deformation between the front wheel and rear wheel. Considering the vehicle suspension dynamics, sprung mass such as tire has a dominant influence on the high frequency response of the suspension system. Because of the limited bandwidth of the actuator in this frequency range, the high frequency response cannot be controlled, so there is no need to accurately estimate the relative velocity of the suspension. Therefore, the difference in tire deformation between the front wheel and the rear wheel does not affect the suspension control method using the proposed estimator. Based on this fact, it can be concluded that it is reasonable to use the wheelbase preview assumption in the proposed estimator for suspension control. Indeed, this wheelbase preview assumption has been used to reduce the number of sensors in many practical areas. For example, several vehicle manufacturers have adopted a sensor system that has wheel acceleration sensors to the front wheels only, since the acceleration of the rear wheels is derived from the front wheel acceleration through the wheelbase preview assumption. Consequently, the additional constraint is derived from wheelbase preview assumption:

$$z_{u2}(t) = z_{u1}\left(t - \tau(t)\right) \tag{2}$$

where $z_{u1,2}$ is the position of the unsprung mass and $\tau = (l_f + l_r)/v_x(t)$ is the time delay.

## III. Relative Velocity Estimation

In this section, the estimation method is introduced in four steps. First, the front suspension force calculation method using a 6-D IMU is proposed. Second, based on the estimated front suspension force, the front suspension relative velocity is derived. Next, the rear suspension relative velocity is derived from the front relative velocity and wheelbase preview assumption. Finally, the rear suspension force is calculated based on the

rear relative velocity and a rear suspension force compensation method using the 6-D IMU is proposed.

### A. Front Suspension Force Calculation

As the first step in estimating the relative velocity, the vertical force applied to the front suspension of the vehicle must be calculated. When the rear suspension force is substituted into the estimated suspension force, the front suspension force is obtained by the governing equation. From (1), the sum of the front suspension force and the difference between the front left and right suspension force are given by

$$F_{L1}(t) + F_{R1}(t) = \frac{1}{l_f + l_r}\left(l_r m_s a_z(t) - I_y \dot{q}(t)\right) \tag{3}$$

$$F_{L1}(t) - F_{R1}(t) = \frac{2}{d} I_x \dot{p}(t) - F_{L2}(t) + F_{R2}(t) \tag{4}$$

Note that the sum of the front suspension force is independent of the rear suspension force. Then, using (3) and (4), each front suspension force can be obtained as

$$F_{L1}(t) = \frac{1}{2}\left\{\frac{1}{l_f + l_r}\left(l_r m_s a_z(t) - I_y \dot{q}(t)\right) + \left(\frac{2}{d} I_x \dot{p}(t) - F_{L2}(t) + F_{R2}(t)\right)\right\} \tag{5}$$

$$F_{R1}(t) = \frac{1}{2}\left\{\frac{1}{l_f + l_r}\left(l_r m_s a_z(t) - I_y \dot{q}(t)\right) - \left(\frac{2}{d} I_x \dot{p}(t) - F_{L2}(t) + F_{R2}(t)\right)\right\} \tag{6}$$

### B. Front Suspension Relative Velocity Estimation

In this section, a force based relative velocity estimation method is introduced. The suspension force is caused by displacement of the suspension spring and damper and can be described as

$$\begin{cases} F_{L1}(t) = k_1 \times \Delta l_{L1}(t) + c_{L1}(t)\Delta \dot{l}_{L1}(t) \\ F_{R1}(t) = k_1 \times \Delta l_{R1}(t) + c_{R1}(t)\Delta \dot{l}_{R1}(t) \end{cases} \tag{7}$$

where $\Delta l_{L1}(t)$ and $\Delta l_{R1}(t)$ are the displacements of the front left and right suspensions. In this paper, the vehicle suspension is controlled by sky-hook damping control algorithm. Therefore, the damping coefficient is described as

$$\begin{cases} c_{L1}(t) = c_{L1n}(t) + c_{L1sky}(t) \\ c_{R1}(t) = c_{R1n}(t) + c_{R1sky}(t) \end{cases} \tag{8}$$

where $c_{L1n}(t)$ and $c_{R1n}(t)$ are the nominal damping coefficient, $c_{L1sky}(t)$ and $c_{R1sky}(t)$ are the sky-hook control inputs. Of course, the vehicle suspension has highly nonlinear characteristics. However, due to complexity, most of the research and algorithms use a linearized vehicle suspension model that requires less computational complexity to implement algorithms in real vehicles[22], [23]. In this study, the nonlinear damper model is approximated to a linear model which ignores the higher order terms and applies a constant nominal damping coefficient. As

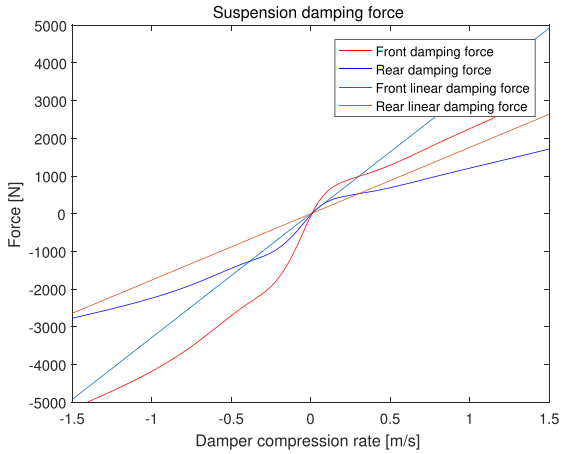


Fig. 2. Nonlinear damping force and linearized damping force.

can be seen in Fig. 2, the actual damping coefficient is approximated by linear damping, resulting in model uncertainty due to linearization. The effect of this damping uncertainty will be addressed in Section V. (7) can be rewritten in state-space form as

$$\begin{pmatrix} \Delta \dot{l}_{L1} \\ \Delta \dot{l}_{R1} \end{pmatrix} = \begin{pmatrix} -k_1/c_{L1} & 0 \\ 0 & -k_1/c_{R1} \end{pmatrix} \begin{pmatrix} \Delta l_{L1} \\ \Delta l_{R1} \end{pmatrix} + \begin{pmatrix} F_{L1}/c_{L1} \\ F_{R1}/c_{R1} \end{pmatrix} \tag{9}$$

This system is two dimensional linear time invariant system. The state of this system is the suspension displacement and the input is the suspension force. Consequently, assuming that the front suspension force is known and the initial condition of this system is calculated based on the 6-D IMU, the suspension relative velocity can be obtained.

### C. Derive the Rear Suspension Information

In the third step of the estimation procedure, the information of the rear suspension is derived. Using relative velocity, the vertical velocity of the unsprung mass is represented as

$$\begin{cases} v_{uL1}(t) = v_{sL1}(t) + \Delta \dot{l}_{L1}(t) \\ v_{uR1}(t) = v_{sR1}(t) + \Delta \dot{l}_{R1}(t) \\ v_{uL2}(t) = v_{sL2}(t) + \Delta \dot{l}_{L2}(t) \\ v_{uR2}(t) = v_{sR2}(t) + \Delta \dot{l}_{R2}(t) \end{cases} \tag{10}$$

The vertical velocities of the sprung mass $v_{sL1,2}(t)$ and $v_{sR1,2}(t)$ can be calculated out of 6-D IMU sensor measurement. From the geometric relationships between the vertical motion of each corner of the vehicle and the vertical motion of the centre of mass[21], the vertical velocity of each corner of the vehicle can be expressed as

$$\begin{cases} v_{sL1}(t) = v_{c.g}(t) - l_f q(t) + \frac{d}{2} p(t) \\ v_{sR1}(t) = v_{c.g}(t) - l_f q(t) - \frac{d}{2} p(t) \\ v_{sL2}(t) = v_{c.g}(t) + l_r q(t) + \frac{d}{2} p(t) \\ v_{sR2}(t) = v_{c.g}(t) + l_r q(t) - \frac{d}{2} p(t) \end{cases} \tag{11}$$

Note that the roll and pitch rate of the sprung mass are included in the sensor measurement. Like other previous studies [24], [25], the vehicle heave velocity $v_{c.g}(t)$ is calculated by integrating the vehicle heave acceleration $a_z(t)$. According to the

wheelbase preview assumption, the vertical velocity of the front suspension is the future information of the vertical velocity of the rear suspension. Therefore, the vertical velocity of the rear unsprung mass can be described by the following equations:

$$\begin{cases} v_{uL2}(t) = v_{uL1}\left(t-\tau(t)\right) \\ v_{uR2}(t) = v_{uR1}\left(t-\tau(t)\right) \end{cases} \tag{12}$$

Finally, according to (10) (12), the relative velocities of the rear suspensions are described as

$$\begin{cases} \Delta\dot{l}_{L2}(t) = V_{uL1}\left(t-\tau(t)\right) - V_{sL2}(t) \\ \Delta\dot{l}_{R2}(t) = V_{uR1}\left(t-\tau(t)\right) - V_{sR2}(t) \end{cases} \tag{13}$$

### D. Rear Suspension Force Calculation and Compensation

In this section, the rear suspension force is calculated and compensated. In addition, the overall estimation scheme is presented. Based on the rear suspension relative velocity, the vertical forces of the rear suspension are given by

$$\begin{cases} F_{L2}(t) = k_2\Delta l_{L2}(t) + c_{L2}(t)\Delta\dot{l}_{L2}(t) \\ F_{R2}(t) = k_2\Delta l_{R2}(t) + c_{R2}(t)\Delta\dot{l}_{R2}(t) \end{cases} \tag{14}$$

Note that (14) is derived from front relative velocities, the wheelbase preview assumption, and sensor measurements. The wheelbase preview assumption provides additional constraints to overcome insufficient governing equations; however, there is a potential problem that the estimation error can be accumulated during the estimation process. Therefore, a certain compensation is required to obtain a more accurate estimate of the rear suspension force. Similar to (3), the sum of the rear force is given as

$$F_{L2}(t) + F_{R2}(t) = \frac{1}{l_f + l_r}\left(l_f m_s a_z(t) + I_y\dot{q}(t)\right) \tag{15}$$

According to (15), the sum of rear left force and rear right force can be determined from the sensor measurements. Thus, using (15), the compensated rear suspension force is given by

$$F_{L2\_comp}(t) = \frac{1}{2}\left\{\frac{1}{l_f + l_r}\left(l_f m_s a_z(t) + I_y\dot{q}(t)\right) + \left(F_{L2}(t) - F_{R2}(t)\right)\right\} \tag{16}$$

$$F_{R2\_comp}(t) = \frac{1}{2}\left\{\frac{1}{l_f + l_r}\left(l_f m_s a_z(t) + I_y\dot{q}(t)\right) - \left(F_{L2}(t) - F_{R2}(t)\right)\right\} \tag{17}$$

where are calculated by (14). Note that always satisfy equation (15). Therefore, the compensated relative velocities of the rear suspensions are given by the same procedure as in (9). Furthermore, the rear suspension forces thus obtained are used to derive the front suspension forces. Finally, the overall estimation scheme is illustrated in Fig. 3.

## IV. Estimator Design and Stability Analysis

This section performs a stability analysis for this closed-loop estimation system. A mathematical description of the overall estimation scheme is given in Section IV-A. Based on this result, a stability analysis for this estimator is conducted in Section IV-B. Consequently, stability is verified numerically using vehicle parameters.

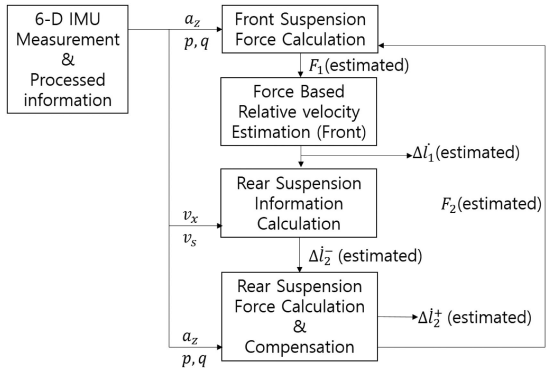


Fig. 3. Overall estimation scheme.

### A. Estimator Description

In this section, the entire estimation method is described mathematically and expressed in state space form. According to (10), (12), and (13), the rear relative velocities are derived from the front ones and sensor measurements. Therefore, (14) is rewritten as

$$\begin{aligned} &F_{L2}(t) \\ &= k_2\left(\int V_{sL1}\left(t-\tau\right)dt + \Delta l_{L1}\left(t-\tau\right) - \int V_{sL2}(t)dt\right) \\ &\quad + c_{L2}\left(V_{sL1}\left(t-\tau\right) + \Delta\dot{l}_{L1}\left(t-\tau\right) - V_{sL2}(t)\right) \end{aligned} \tag{18}$$

$$\begin{aligned} &F_{R2}(t) \\ &= k_2\left(\int V_{sR1}\left(t-\tau\right)dt + \Delta l_{R1}\left(t-\tau\right) - \int V_{sR2}(t)dt\right) \\ &\quad + c_{R2}\left(V_{sR1}\left(t-\tau\right) + \Delta\dot{l}_{R1}\left(t-\tau\right) - V_{sR2}(t)\right) \end{aligned} \tag{19}$$

Note that the rear suspension forces are used to calculate the front ones and the front relative velocities are derived from the front suspension forces. Therefore, using (9),(18) and (19) the front relative velocities are defined as the superposition of feedback terms and sensor measurement terms. This equation then can be rewritten in the state space form:

$$\begin{aligned} \begin{pmatrix} \Delta\dot{l}_{L1} \\ \Delta\dot{l}_{R1} \end{pmatrix}(t) &= \begin{pmatrix} -k_1/c_{L1} & 0 \\ 0 & -k_1/c_{R1} \end{pmatrix}\begin{pmatrix} \Delta l_{L1} \\ \Delta l_{R1} \end{pmatrix}(t) \\ &+ \begin{pmatrix} -k_2/2c_{L1} & k_2/2c_{L1} \\ k_2/2c_{R1} & -k_2/2c_{R1} \end{pmatrix}\begin{pmatrix} \Delta l_{L1} \\ \Delta l_{R1} \end{pmatrix}(t-\tau) \\ &+ \begin{pmatrix} -c_{L2}/2c_{L1} & c_{R2}/2c_{L1} \\ c_{L2}/2c_{R1} & -c_{R2}/2c_{R1} \end{pmatrix}\begin{pmatrix} \Delta\dot{l}_{L1} \\ \Delta\dot{l}_{R1} \end{pmatrix}(t-\tau) + \Gamma(t,\tau) \end{aligned} \tag{20}$$

where $\Gamma(t,\tau)$ is sensor measurement term. Consequently, the estimation algorithm is a linear neutral type delay system

(NTDS) [26], [27]:

$$\dot{x}(t) = Ax(t) + A_d x\left(t-\tau(t)\right) + J\dot{x}\left(t-\tau(t)\right) + \Gamma\left(t,\tau\right) \tag{21}$$

where $x = (\Delta l_{L1}\ \Delta l_{R1})^T$ and

$$A = \begin{pmatrix} -k_1/c_{L1} & 0 \\ 0 & -k_1/c_{R1} \end{pmatrix}$$

$$A_d = \begin{pmatrix} -k_2/2c_{L1} & k_2/2c_{L1} \\ k_2/2c_{R1} & -k_2/2c_{R1} \end{pmatrix}$$

$$J = \begin{pmatrix} -c_{L2}/2c_{L1} & c_{R2}/2c_{L1} \\ c_{L2}/2c_{R1} & -c_{R2}/2c_{R1} \end{pmatrix}$$

Using the system model (21), the NTDS state observer can be designed. According to previous studies about NTDS observer [28], [29], the linear observer is designed in the following form:

$$\begin{aligned}\dot{\hat{x}}(t) = {} & A\hat{x}(t) + A_d\hat{x}\left(t-\tau(t)\right) + J\dot{\hat{x}}\left(t-\tau(t)\right) \\ & + K\left[y(t) - \hat{y}(t)\right] + \Gamma\left(t,\tau\right)\end{aligned} \tag{22}$$

where the constant matrix $K$ is the observer gain with an appropriate dimension. According to (3) and (15), summation of the front vertical suspension force can be derived from 6-D IMU measurement. Therefore, this physical parameter can be another form of system measurement. Consequently, the system measurement:

$$\begin{aligned}y(t) = {} & C_1^0 x(t) + C_2^0\dot{x}(t) + C_1^J x\left(t-\tau(t)\right) \\ & + C_2^J\dot{x}\left(t-\tau(t)\right) + \gamma(t)\end{aligned} \tag{23}$$

where $\gamma(t)$ is another sensor measurement term and

$$C_1^0 = \begin{pmatrix} k_1 & k_1 \\ 0 & 0 \end{pmatrix},\ C_2^0 = \begin{pmatrix} c_{L1} & c_{R1} \\ 0 & 0 \end{pmatrix}$$

$$C_1^J = \begin{pmatrix} 0 & 0 \\ k_2 & k_2 \end{pmatrix},\ C_2^J = \begin{pmatrix} 0 & 0 \\ c_{L2} & c_{R2} \end{pmatrix}$$

Let the error state is $e(t) = x(t) - \hat{x}(t)$, then according to (21), (22) and (23), the error dynamics can be derived as

$$\dot{e}(t) = \bar{A}e(t) + \bar{A}_d e\left(t-\tau(t)\right) + \bar{J}\dot{e}\left(t-\tau(t)\right) \tag{24}$$

where $\bar{A} = (I + KC_2^0)^{-1}(A - KC_1^0)$, $\bar{A}_d = (I + KC_2^0)^{-1}(A_d - KC_1^J)$ and $\bar{J} = (I + KC_2^0)^{-1}(J - KC_2^J)$.

### *B. NTDS Observer Stability Analysis*

Note that the overall estimation algorithm has NTDS characteristics. The stability of NTDS has been studied during the past four decades [30]–[40]. Since the time delay in the estimation method is varying depending on the vehicle velocity, the delay-independent stability criterion is suitable to verify the stability of the estimation method. Stability theory based on the Liapunov-Krasovskii functional [31], [39], [40] is mainly used as a method of proving delay independent stability. Assuming that $\Gamma(t,\tau)$ is bounded using a signal filtering technique such as high pass filtering, the stability of error dynamics (24) is verified by the following theorem [31], [39].

Theorem 1: The NTDS error dynamics (24) is delay-independent asymptotic stable if

- $\bar{A}$ is a Hurwitz
- The spectral radius of $\bar{J}$ is less than one
- There exist two symmetric and positive definite matrixes $R > 0$ and $Q > 0$ such that the following Riccati equation has a symmetric and positive definite solution $P > 0$:

$$\begin{aligned}\bar{A}^T P + P\bar{A} - \left[P\left(\bar{A}\bar{J} + \bar{A}_d\right) + S\bar{J}\right] R^{-1} \\ \times \left[\bar{J}^T S + \left(\bar{A}_d^T + \bar{J}^T\bar{A}^T\right)P\right] + Q + S = 0\end{aligned} \tag{25}$$

where $S > 0$ is the symmetric and positive definite solution of the Lyapunov discrete equation:

$$\bar{J}^T S\bar{J} - S + R = 0 \tag{26}$$

Now the stability of the estimation algorithm can be verified using this theorem. To reduce complexity, it is assumed that the damping coefficient on the left is the same as the damping coefficient on the right. Therefore, $c_{L1} = c_{R1} = c_1$ and $c_{L2} = c_{R2} = c_2$. The observer gain $K$ is designed to make $(I + KC_2^0)$ is non-singular. First the eigenvalue of $\bar{A}$ is given by

$$\lambda\left(\bar{A}\right) = -k_1/c_1, -k_1/c_1 \tag{27}$$

Since $\bar{A}$ always has a negative eigenvalue, $\bar{A}$ is always Hurwitz. Second, the eigenvalue of $\bar{J}$ is given by

$$\lambda\left(\bar{J}\right) = -c_2/c_1, -\frac{c_2K_{12} + c_2K_{22}}{c_1K_{11} + c_1K_{21} + 1} \tag{28}$$

Note that most vehicles have front damping that is larger than rear one. Therefore, the spectral radius of $\bar{J}$ is less than one. Using the vehicle parameters, observer gain $K = (0.001\ 0.001;0.001\ 0.001)$ and the nominal damping coefficient ($c_1 =$ 3286.8 Ns/m, $c_2 =$ 1761.6 Ns/m), then the solution of (25) is given by

$$P = \begin{pmatrix} 0.0202 & 0.005 \\ 0.005 & 0.0202 \end{pmatrix} \tag{29}$$

Since $P$ is positive definite, the error dynamics is stable.

## V. Simulation

In this section, the sky-hook control simulation based on the proposed estimation method is performed. The two-state damper sky-hook control law[10], [11] widely used in the practical areas is given by

$$\begin{cases} c_{sky}(t) = c_{\max} & if\ \ v_s(t)(v_s(t) - v_u(t)) \geq 0 \\ c_{sky}(t) = c_{\min} & if\ v_s(t)(v_s(t) - v_u(t)) < 0 \end{cases} \tag{30}$$

$$\dot{c}(t) = -\beta c(t) + \beta c_{sky}(t) + c_n \tag{31}$$

where $c_{sky}(t)$, $c(t)$ and $c_n(t)$ are the damping command, the actual damping coefficient of the suspension and the nominal damping of the suspension. Since the suspension actuator has a bandwidth in real world, the actuator dynamics is represented by (31). In this simulation, the actuator bandwidth $\beta$ is set to $30\pi$ Note that this control law requires the information about the suspension relative velocity. To verify the proposed estimation method, the frequency and time response analysis of the

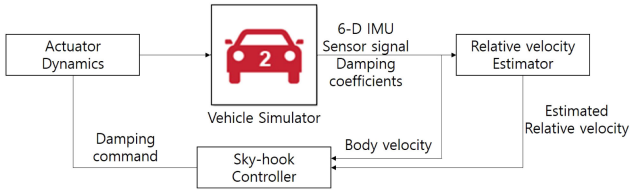


Fig. 4. Overall simulation scheme.

TABLE II
VEHICLE SIMULATION PARAMETERS

| Parametric uncertainty | Variation |
|---|---|
| $m_s$ | 1370+30% kg |
| $I_x$ | 671.3+20% $kgm^2$ |
| $I_y$ | 1972.8+20% $kgm^2$ |
| $c_{max1}$ | 14000 Ns/m |
| $c_{min1}$ | 1700 Ns/m |
| $c_{max2}$ | 6100 Ns/m |
| $c_{min2}$ | 920 Ns/m |

TABLE III
TIME RESPONSE SIMULATION SCENARIOS

| Case | Maneuver | Longitudinal velocity |
|---|---|---|
| 1 | Sinusoidal road | 35km/h |
| 2 | Speed bump | 30km/h |
| 3 | Half Speed bump(Left side) | 30km/h |
| 4 | Potholes(Left side) | 120 to 25km/h |

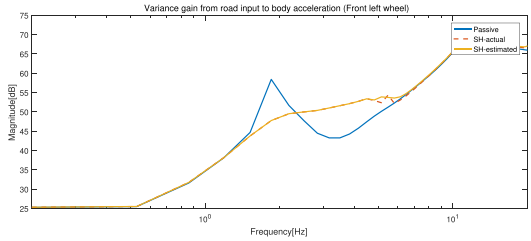


Fig. 5. Frequency response from front left road elevation to front left body acceleration.

sky-hook controller based on the estimated relative velocity is performed. Since the closed-loop control system is nonlinear, the variance gain is computed to describe the frequency response. Finally, the overall simulation scheme is illustrated in Fig. 4.

### A. Simulation Set-Up

To verify the proposed estimation method, Carsim and Matlab & Simulink were used, which are used widely to develop vehicle control systems in many practical areas. In this paper, D-class sedan model is used to verify the proposed algorithm. Because Carsim is a highly nonlinear black box model, it also includes many vehicle nonlinearities not covered in this paper. Additional parametric uncertainties given in Table II and initial condition error were applied to the estimator to simulate the environment closer to the experiments with real production vehicles. In addition, the longitudinal velocity of the vehicle has an error of 1.38m/s, which is equal to 5km/h. This error value usually occurs when vehicles longitudinal velocity is estimated using the wheel velocity. This simulation was performed assuming that a 6-D IMU was attached to the centre of mass of the vehicle body. The 6-D IMU sensor measurements include measurement noise designed with reference to the gyroscope ADW22307 and accelerometer ADXL103 data sheet. Coordinate transformation of sensor measurements is also an important part of the real world, but is not considered in this study. In addition, three sprung mass accelerometers and two unsprung mass accelerometers is configured to compare the proposed algorithm with another algorithm using different sensor measurements. In general, most of the automotive manufacturers use these five sensors to estimate the relative velocity of each corner of a vehicle suspension. In this paper, an integration-based estimator that is widely used in practical fields is used. To compare the performance of the algorithms, an integrator with a second order highpass filter with a cut off frequency of 0.4 rad/s is used [18].

The simulation analysis is performed as follows. First, the frequency response of the estimator based sky-hook controller is analysed. On a sinusoidal road surface which has the road wavelength matched the vehicle wheelbase, the frequency response from 0.2 Hz to 20 Hz is explored. Next the road surfaces used for the time response simulations were selected from the typical road surfaces, which are mainly used for evaluating the ride quality of production vehicles. Case 1, a low frequency sinusoidal road surface with an elevation of 0.02 meter to 0.10 meter, was used to estimate the low frequency performance of the estimator based controller. Second, a 3.6m×0.1m speed bump was used to evaluate the performance of the estimator where unsprung mass motion is dominant. Next, a half-bump test was performed in which the vehicle passes through the same speed bump only to the left half of a vehicle to cause severe vehicle roll motion. Finally, potholes test in which the decelerating vehicle passes through the two potholes is performed to investigate the effect of braking and sudden unsprung mass motion on the proposed estimation algorithm. Table III summarizes the time response simulation scenarios to verify the estimator performance.

### B. Frequency Response Simulation Result

Fig. 5 shows the result of sinusoidal road simulation. Note that this figure shows the typical frequency response of vehicle suspension dynamics. Around 2 Hz, the first peak appears in the passive suspension frequency response. This peak can be suppressed using the suspension control. According to this figure, this peak response is suppressed in both the actual relative velocity based sky-hook control response and the estimated relative velocity based sky-hook control response. The second peak that appears at approximately 12 Hz cannot be suppressed since this peak is located on invariant frequency. It is noteworthy that the actual relative velocity based sky-hook control response and the estimated relative velocity based sky-hook control response show almost the same frequency response. This result shows that the proposed estimator can replace the estimation method using accelerometers located in sprung mass and unsprung mass.

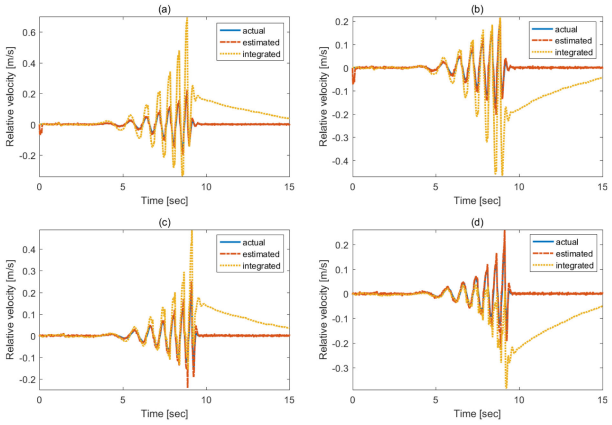


Fig. 6. Sinusoidal road simulation results for relative velocity estimation: (a) Front left suspension relative velocity. (b) Front right suspension relative velocity. (c) Rear left suspension relative velocity. (d) Rear right suspension relative velocity.

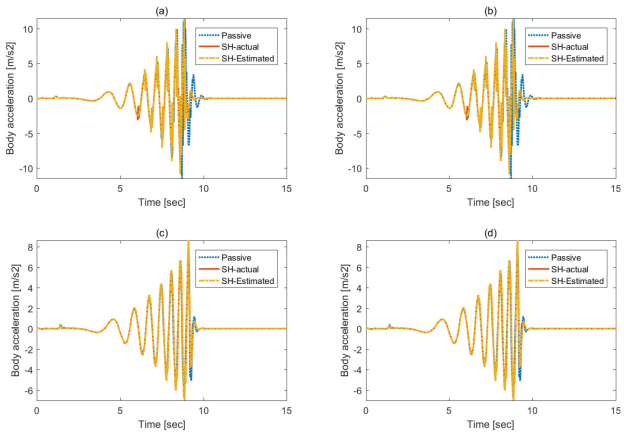


Fig. 7. Sinusoidal road simulation results for body acceleration: (a) Front left body acceleration. (b) Front right body acceleration. (c) Rear left body acceleration. (d) Rear right body acceleration.

## C. Time Response Simulation Results

*1) Case 1. Sinusoidal Road Simulation:* Fig. 6 shows the results of sinusoidal road simulation. Since the vehicle had longitudinal velocity on a symmetrical road surface, the roll motion of the vehicle was negligibly small. Therefore, according to (5) and (6), the estimated rear suspension forces did not have an impact on front suspension force estimation. As a result, the front suspension forces of each side can be obtained from 6-D IMU measurements. Likewise, the rear suspension forces of each side are calculated from (15). Due to the parametric uncertainties and the linear approximated suspension model, the estimation errors are increased accordingly the magnitude of relative velocities is increased. However, the phase of the estimated relative velocity is the same as the phase of the actual ones. Since NTDS observer is asymptotically stable, the initial condition error converges to zero. Compared with the integrator-based estimator, the proposed estimator converges more accurately and quickly. According to the simulation results, the drifting issue caused by accumulated error and sensor noise occurs and this phenomenon is a typical problem that can be found in integrator-based estimator. Fig. 7 shows the results of estimated relative velocity based sky-hook control. This figure shows that the body acceleration controlled by the estimated relative velocity based sky-hook controller is the same as the body acceleration controlled by the actual relative velocity based sky-hook controller. This simulation result implies the proposed method can replace conventional estimation method using accelerometers.

*2) Case 2. Speed Bump Simulation:* When the vehicle is crossing a speed bump, motion of the unsprung mass is more dominant than that of the sprung mass. Since the 6-D IMU sensor is attached on the vehicle body, the movement of the unsprung mass cannot be detected independently. However, this estimation algorithm is based on the suspension forces and they are estimated immediately. Therefore, it is expected that the relative velocities can be estimated for an unsprung mass-motion dominant situation such as speed bump crossing. As in Fig. 8, the relative velocity can still be obtained when the movement of the

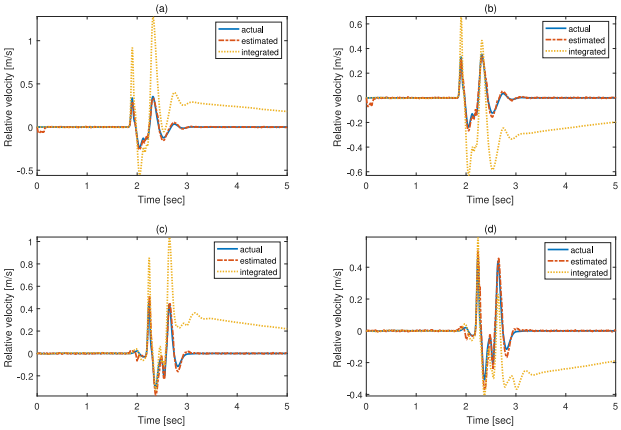


Fig. 8. Speed bump simulation results for relative velocity estimation: (a) Front left suspension relative velocity. (b) Front right suspension relative velocity. (c) Rear left suspension relative velocity. (d) Rear right suspension relative velocity.

unsprung mass is more dominant than that of the sprung mass. Since the tire does not touch the road surface, high frequency relative velocity estimation error occurs in 2.3 seconds. However, according to Fig. 9, there is comparatively high estimation error, but the vehicle acceleration results of both control methods are the same. Because of the actuator bandwidth, high frequency estimation errors do not affect suspension control in the real world. As with case 1, the proposed estimator has more robust performance than the integrator-based estimator with drifting issue. In conclusion, the proposed estimation method is also suitable for the motion of an unsprung mass dominant situation such as a speed bump crossing.

In case 1 and case 2, there is no roll motion of the vehicle, and the error is caused sorely by parametric uncertainties since the estimated rear suspension forces do not affect the front suspension force estimation.

*3) Case 3. Half Bump Simulation:* Some drivers try to pass over speed bumps with only one side of the vehicle. This half bump maneuver is therefore a major test scenario for evaluating the ride comfort in a practical area. In this scenario, the estimated

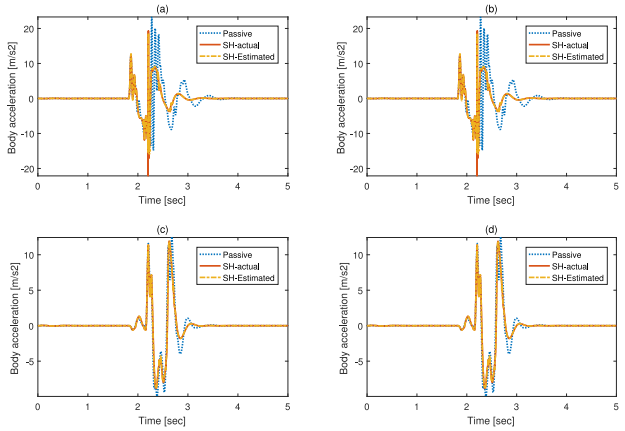


Fig. 9. Speed bump simulation results for body acceleration: (a) Front left body acceleration. (b) Front right body acceleration. (c) Rear left body acceleration. (d) Rear right body acceleration.

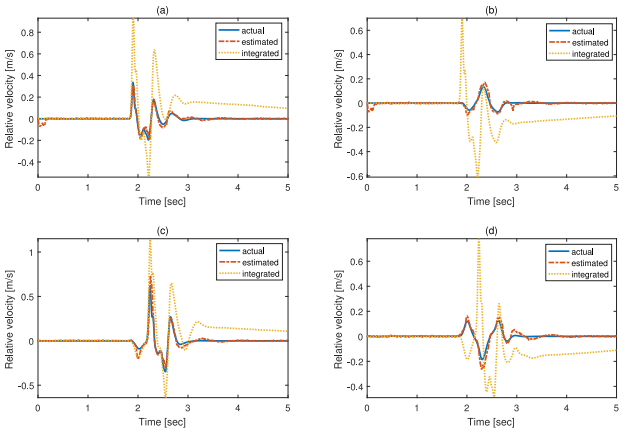


Fig. 10. Half bump simulation results for relative velocity estimation: (a) Front left suspension relative velocity. (b) Front right suspension relative velocity. (c) Rear left suspension relative velocity. (d) Rear right suspension relative velocity.

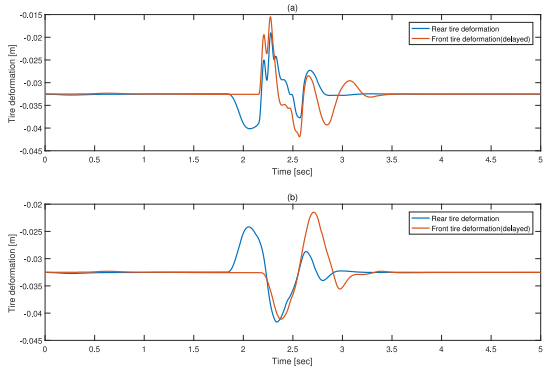


Fig. 11. Comparison of the front and rear tire deformation: (a) Left side tire deformation. (b) Right side tire deformation.

TABLE IV
ERRORS OF THE SUSPENSION RELATIVE VELOCITY ESTIMATION

| Case | | $e_{max}$ | $e_{rms}$ | $\sigma^2$ |
|---|---|---|---|---|
| Case 1 | Front left | 0.0821 | 0.0102 | 8.7531e-05 |
| | Front right | 0.0938 | 0.0107 | 8.8912e-05 |
| | Rear left | 0.1027 | 0.0099 | 1.0013e-04 |
| | Rear right | 0.0997 | 0.0100 | 9.5989e-05 |
| Case 2 | Front left | 0.0975 | 0.0182 | 2.3322e-04 |
| | Front right | 0.0725 | 0.0149 | 2.2397e-04 |
| | Rear left | 0.1778 | 0.0303 | 5.4074e-04 |
| | Rear right | 0.1989 | 0.0220 | 5.5937e-04 |
| Case 3 | Front left | 0.0963 | 0.0183 | 2.6310e-04 |
| | Front right | 0.0726 | 0.0341 | 2.2903e-04 |
| | Rear left | 0.3103 | 0.0148 | 9.6598e-04 |
| | Rear right | 0.0842 | 0.0188 | 3.1240e-04 |
| Case 4 | Front left | 0.0963 | 0.0550 | 0.0030 |
| | Front right | 0.1716 | 0.0853 | 0.0073 |
| | Rear left | 0.7608 | 0.0234 | 5.4057e-04 |
| | Rear right | 0.1800 | 0.0244 | 5.9263e-04 |

rear suspension forces have an impact on calculating the front suspension forces since the vehicle has roll motion. Therefore, it can be expected that the estimation error is increased more than in other maneuvers where the vehicle does not have roll motion.

Fig. 11 shows the tire deformation difference between the front wheels and the rear ones. This estimation algorithm is based on the wheelbase preview assumption. In order to perfectly apply the wheelbase preview assumption accurately, the delayed tire deformation of the front wheels needs to be matched to the rear tire deformation perfectly. However, due to other characteristics such as sprung mass, damping coefficient, spring stiffness, and tire characteristics between the front wheels and rear wheels, the wheelbase preview assumption is corrupted. Therefore, an additional estimation error is occurred associated with the tire deformation difference between the front and the rear ones. According to Fig. 10 and Table IV, the absolute magnitude of the estimation error is increased more than in other cases where the vehicle has no roll motion, but the phase of the estimated relative velocities are the same as the phase of the actual ones. As a result, it was verified that the suspension relative velocity can be obtained using a 6-D IMU attached to the vehicle chassis. Compared to the integrator-based estimator, in addition to the drifting issue, the difference in performance is noticeable on the right side of the vehicle that does not cross the speed bump. This result indicates that signal loss due to high pass filtering affects the estimation of low relative velocity regions. Based on this simulation, it can be expected that the proposed estimation method can be used to suspension control for the roll motion dominant maneuver such as half bump crossing. Fig. 12 shows the time response of the body acceleration and this simulation results denote that this expectation is correct.

*4) Case 4. Potholes Simulation:* Pothole which shown on asphalt pavement is a main cause of ride quality reduction. Moreover, an accident may occur since a high speed vehicle decelerate to avoid a pothole. To verify the performance of the proposed estimation algorithm in such road conditions, a potholes road simulation is performed. In this paper, a simulation is performed in which the vehicle crosses two potholes on the left side. In addition, to simulate the drivers reaction on the pothole road, the vehicle was given an additional brake input.

According to Fig. 13 and Table IV, a relatively high estimation error occurs in comparison with the other cases. As mentioned in the case 3, the rolling motion of the vehicle and the

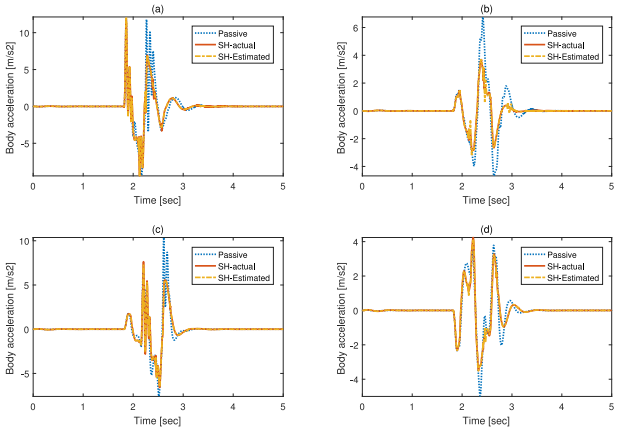


Fig. 12. Half bump simulation results for body acceleration: (a) Front left body acceleration. (b) Front right body acceleration. (c) Rear left body acceleration. (d) Rear right body acceleration.

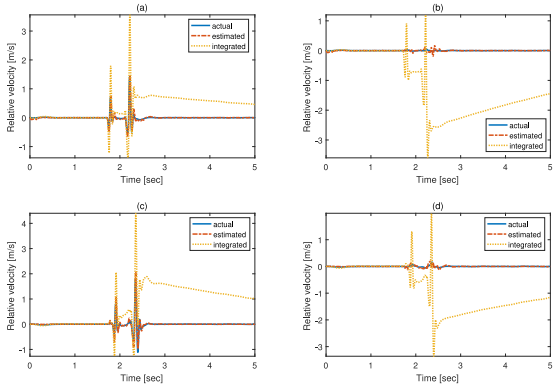


Fig. 13. Potholes simulation results for relative velocity estimation: (a) Front left suspension relative velocity. (b) Front right suspension relative velocity. (c) Rear left suspension relative velocity. (d) Rear right suspension relative velocity.

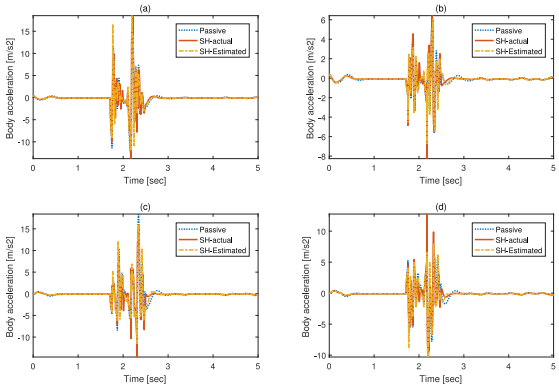


Fig. 14. Potholes simulation results for body acceleration: (a) Front left body acceleration. (b) Front right body acceleration. (c) Rear left body acceleration. (d) Rear right body acceleration.

tire deformation due to the sudden change of the road surface affect the relative velocity estimation. Moreover, as the relative velocity of the suspension increases, the estimation error due to model uncertainties increases. Compared to the integrator-based estimator, however, very little phase error is occurred and the magnitude of the relative velocity is relatively accurate. According to the simulation results, the bias of the vertical acceleration due to braking has no effect on the state estimation. It is noteworthy that passive suspension and controlled semi-active suspension make little difference in performance evaluation based on body acceleration. Fig. 14 shows the characteristics of a semi-active suspension control using a sky-hook algorithm that cannot improve the performance of the high-frequency region. In conclusion, the relative velocity of the suspension is estimated with a small phase error, there is no performance improvement over passive suspension due to the limitations of the control algorithm and actuator bandwidth.

## VI. Conclusion

In this paper, a method of estimating the suspension relative velocity using a single 6-D IMU attached to the vehicle body is proposed. Based on the wheelbase preview assumption, this estimation method provides the suspension relative velocity on various road surfaces. The proposed estimation algorithm is consisted of a closed-loop system. Since this system is described as NTDS, the stability criterion of NTDS is used to verify the delay independent stability of this estimator. Therefore, the estimator has robust performance against initial condition error. In this paper, using the vehicle simulator Carsim, a simulational verification is performed on various scenarios. Although the estimation method is proposed based on the approximated linear model, the simulation results show that this estimator provides a reasonable estimation of the suspension relative velocity using a sensor attached to the vehicle body. It is worth noting that even though this estimator has estimation error caused by parameter uncertainty and tire deformation, very little phase error is occurred. Therefore, this estimator can be used for vehicle suspension control applications. Another advantage of the proposed estimation method is that the problem of sensor packaging can be solved, and the number of sensors and costs can also be reduced. In conclusion, using the proposed estimation method, the suspension relative velocity can be obtained with good robustness while reducing the system cost and installation efforts at the same time.

## References

[1] R. Rajamani, *Vehicle Dynamics and Control*. Berlin, Germany: Springer Science & Business Media, 2011.
[2] R. Rajamani and J. Hedrick, "Performance of active automotive suspensions with hydraulic actuators: Theory and experiment," in *Proc. IEEE Amer. Control Conf.*, 1994, pp. 1214–1218.
[3] T. Butsuen, "The design of semi-active suspensions for automotive vehicles," Ph.D. dissertation, Dept. Mech. Eng., Massachusetts Inst. Technol., Cambridge, MA, USA, 1989.
[4] J. Swevers, C. Lauwerys, B. Vandersmissen, M. Maes, K. Reybrouck, and P. Sas, "A model-free control structure for the on-line tuning of the semi-active suspension of a passenger car," *Mech. Syst. Signal Process.*, vol. 21, no. 3, pp. 1422–1436, 2007.
[5] S. M. Savaresi and C. Spelta, "A single-sensor control strategy for semi-active suspensions," *IEEE Trans. Control Syst. Technol.*, vol. 17, no. 1, pp. 143–152, Jan. 2009.
[6] H.-S. Roh and Y. Park, "Preview control of active vehicle suspensions based on a state and input estimator," SAE Technical Paper, Warrendale, PA, USA, Tech. Rep. 1336, 1998.
[7] D. Karnopp, M. J. Crosby, and R. Harwood, "Vibration control using semi-active force generators," *J. Eng. Industry*, vol. 96, no. 2, pp. 619–626, 1974.

[8] R. Darus and Y. M. Sam, "Modeling and control active suspension system for a full car model," in *Proc. IEEE 5th Int. Colloquium Signal Process. Appl.,* 2009, pp. 13–18.
[9] H.-S. Roh and Y. Park, "Observer-based wheelbase preview control of active vehicle suspensions," *KSME Int. J.*, vol. 12, no. 5, pp. 782–791, 1998.
[10] S. M. Savaresi, E. Silani, and S. Bittanti, "Acceleration-driven-damper (add): An optimal control algorithm for comfort-oriented semiactive suspensions," *J. Dyn. Syst., Meas. Control*, vol. 127, no. 2, pp. 218–229, 2005.
[11] S. M. Savaresi and C. Spelta, "Mixed sky-hook and add: Approaching the filtering limits of a semi-active suspension," *J. Dyn. Syst., Meas. Control*, vol. 129, no. 4, pp. 382–392, 2007.
[12] K. Yi and B. Suk Song, "Observer design for semi-active suspension control," *Vehicle Syst. Dyn.*, vol. 32, no. 2/3, pp. 129–148, 1999.
[13] K. Yi, "Design of disturbance decoupled bilinear observers," *KSME J.*, vol. 9, no. 3, pp. 344–350, 1995.
[14] L. Dugard, O. Sename, S. Aubouet, and B. Talon, "Full vertical car observer design methodology for suspension control applications," *Control Eng. Pract.*, vol. 20, no. 9, pp. 832–845, 2012.
[15] R. K. Dixit and G. D. Buckner, "Sliding mode observation and control for semiactive vehicle suspensions," *Vehicle Syst. Dyn.*, vol. 43, no. 2, pp. 83–105, 2005.
[16] S. Irmscher and E. Hees, "Experience in semi-active damping with state estimators," in *Proc. Annu. Workshop Audio/Vis. Emotion Challenge*, 1996, vol. 96, pp. 193–206.
[17] O. Lindgärde, "Kalman filtering in semi-active suspension control," in *Proc. 15th IFAC World Congr.*, 2002, pp. 1539–1544.
[18] D. Hernandez-Alcantara, L. Amezquita-Brooks, and R. Morales-Menendez, "State-observers for semi-active suspension control applications with low sensitivity to unknown road surfaces," SAE Technical Paper, Warrendale, PA, USA, Tech. Rep. 0867, 2014.
[19] A. Kruczek and A. Stribrsky, "A full-car model for active suspension-some practical aspects," in *Proc. IEEE Int. Conf. Mechatronics*, 2004, vol. 4, pp. 41–45.
[20] C. Kim and P. I. Ro, "An accurate full car ride model using model reducing techniques," *J. Mech. Des.*, vol. 124, no. 4, pp. 697–705, 2002.
[21] J. Kim and H. Lee, "Sensor fault detection and isolation algorithm for a continuous damping control system," *Proc. Institution Mech. Eng., D, J. Automobile Eng.*, vol. 225, no. 10, pp. 1347–1364, 2011.
[22] D. S. Joo, N. Al-Holou, J. M. Weaver, T. Lahdhiri, and F. Al-Abbas, "Nonlinear modeling of vehicle suspension system," in *Proc. IEEE Amer. Control Conf.*, 2000, vol. 1, no. 6, pp. 115–119.
[23] I. Szaszi, P. Gáspár, and J. Bokor, "Nonlinear active suspension modelling using linear parameter varying approach," in *Proc. 10th Mediterranean Conf. Control Autom.*, 2002, pp. 1–10.
[24] W. Kim, J. Lee, S. Yoon, and D. Kim, "Development of mando's new continuously controlled semi-active suspension system," SAE Technical Paper, Warrendale, PA, USA, Tech. Rep. 1721, 2005.
[25] A. Chamseddine and H. Noura, "Control and sensor fault tolerance of vehicle active suspension," *IEEE Trans. Control Syst. Technol.*, vol. 16, no. 3, pp. 416–433, May 2008.
[26] K. Gu and S.-I. Niculescu, "Survey on recent results in the stability and control of time-delay systems," *J. Dyn. Syst., Meas. Control*, vol. 125, no. 2, pp. 158–165, 2003.
[27] J.-P. Richard, "Time-delay systems: An overview of some recent advances and open problems," *Automatica*, vol. 39, no. 10, pp. 1667–1694, 2003.
[28] Z. Wang, J. Lam, and K. J. Burnham, "Stability analysis and observer design for neutral delay systems," *IEEE Trans. Autom. Control*, vol. 47, no. 3, pp. 478–483, Mar. 2002.
[29] B. Chen, J. Lam, and Z. Wang, "Observer design and stabilization for linear neutral delay systems," *ISA Trans.*, vol. 44, no. 1, pp. 35–42, 2005.
[30] M. A. Cruz and J. K. Hale, "Stability of functional differential equations of neutral type," *J. Differ. Equ.*, vol. 7, no. 2, pp. 334–355, 1970.
[31] E. Fridman, "New Lyapunov–Krasovskii functionals for stability of linear retarded and neutral type systems," *Syst. Control Lett.*, vol. 43, no. 4, pp. 309–319, 2001.
[32] M. A. Gomez, A. V. Egorov, and S. Mondié, "Necessary stability conditions for neutral type systems with a single delay," *IEEE Trans. Autom. Control*, vol. 62, no. 9, pp. 4691–4697, Sep. 2017.
[33] G.-D. Hu and G.-D. Hu, "Some simple criteria for stability of neutral delay-differential systems," *Appl. Math. Comput.*, vol. 80, no. 2/3, pp. 257–271, 1996.
[34] V. B. Kolmanovskii, "On the Liapunov–Krasovskii functionals for stability analysis of linear delay systems," *Int. J. Control*, vol. 72, no. 4, pp. 374–384, 1999.
[35] L.-M. Li, "Stability of linear neutral delay-differential systems," *Bull. Australian Math. Soc.*, vol. 38, no. 3, pp. 339–344, 1988.
[36] X. Liao, G. Chen, and E. N. Sanchez, "Delay-dependent exponential stability analysis of delayed neural networks: an LMI approach," *Neural Netw.*, vol. 15, no. 7, pp. 855–866, 2002.
[37] N. Olgac and R. Sipahi, "An exact method for the stability analysis of time-delayed linear time-invariant (LTI) systems," *IEEE Trans. Autom. Control*, vol. 47, no. 5, pp. 793–797, May 2002.
[38] N. Olgac and R. Sipahi, "A practical method for analyzing the stability of neutral type LTI-time delayed systems," *Automatica*, vol. 40, no. 5, pp. 847–853, 2004.
[39] E. I. Verriest and S.-I. Niculescu, "Delay-independent stability of linear neutral systems: A Riccati equation approach," in *Stability and Control of Time-Delay Systems*. Berlin, Germany: Springer, 1998, pp. 92–100.
[40] H. Wenzhang, "Generalization of Liapunov's theorem in a linear delay system," *J. Math. Anal. Appl.*, vol. 142, no. 1, pp. 83–94, 1989.

**Kicheol Jeong** received the B.S. degree in mechanical engineering from Hanyang University, Busan, South Korea, and the M.S. degree in mechanical engineering from the Korea Advanced Institute of Science and Technology (KAIST), Daejeon, South Korea, in 2015 and 2017, respectively. Currently he is working toward the Ph.D. degree in mechanical engineering with KAIST. His research interests include vehicle dynamics and control, fault diagnosis and control theory.

**Seibum B. Choi** received the B.S. degree in mechanical engineering from Seoul National University, Seoul, South Korea, the M.S. degree in mechanical engineering from the Korea Advanced Institute of Science and Technology (KAIST), Seoul, South Korea, and the Ph.D. degree in controls from the University of California, Berkeley, Berkeley, CA, USA, in 1993. Since 2006, he has been with the faculty of the Mechanical Engineering Department with KAIST. His research interests include fuel saving technology, vehicle dynamics and control, and application of self-energizing mechanism.